

Investigation of 3-fragment photodissociation of O₃ at 193.4 and 157.6 nm by coincident measurements

Mikhail Ryazanov, Aaron W. Harrison, Gregory Wang, Paul E. Crider, and Daniel M. Neumark

Citation: *The Journal of Chemical Physics* **140**, 234304 (2014); doi: 10.1063/1.4882644

View online: <http://dx.doi.org/10.1063/1.4882644>

View Table of Contents: <http://scitation.aip.org/content/aip/journal/jcp/140/23?ver=pdfcov>

Published by the [AIP Publishing](#)

Articles you may be interested in

[Oxygen cluster anions revisited: Solvent-mediated dissociation of the core O₄⁻ anion](#)
J. Chem. Phys. **136**, 094312 (2012); 10.1063/1.3691104

[Interpretation of the photoelectron spectra of superalkali species: Li₃O and Li₃O⁺](#)
J. Chem. Phys. **135**, 164307 (2011); 10.1063/1.3636082

[Photolysis of pure solid O₃ and O₂ films at 193 nm](#)
J. Chem. Phys. **134**, 194501 (2011); 10.1063/1.3589201

[Production of O₂ Herzberg states in the deep UV photodissociation of ozone](#)
J. Chem. Phys. **131**, 011101 (2009); 10.1063/1.3157236

[The photodissociation dynamics of ozone at 226 and 248 nm : O \(P J 3 \) atomic angular momentum polarization](#)
J. Chem. Phys. **127**, 144304 (2007); 10.1063/1.2790890



Re-register for Table of Content Alerts

Create a profile.



Sign up today!



Investigation of 3-fragment photodissociation of O₃ at 193.4 and 157.6 nm by coincident measurements

Mikhail Ryazanov, Aaron W. Harrison, Gregory Wang, Paul E. Crider,^{a)}
and Daniel M. Neumark^{b)}

*Department of Chemistry, University of California, Berkeley, California 94720, USA
and Chemical Sciences Division, Lawrence Berkeley National Laboratory, Berkeley, California 94720, USA*

(Received 23 April 2014; accepted 29 May 2014; published online 16 June 2014)

Photodissociation of the ozone molecule at 193.4 nm (6.41 eV) and 157.6 nm (7.87 eV) is studied by fast-beam translational spectroscopy. Coincident detection of the dissociation products allows direct observation of the 3-fragment channel and determination of its kinematic parameters. The results indicate that at each wavelength, 3-fragment dissociation proceeds through synchronous concerted bond breaking, but the energy partitioning among the fragments is different. The branching fraction of the 3-fragment channel increases from 5.2(6)% at 193.4 nm to 26(4)% at 157.6 nm, in agreement with previous studies. It is shown that vibrational excitation of the symmetric stretch mode in O₃ molecules created by photodetachment of O₃⁻ anion enhances the absorption efficiency, especially at 193.4 nm, but does not have a strong effect on the 3-fragment dissociation. © 2014 AIP Publishing LLC. [<http://dx.doi.org/10.1063/1.4882644>]

I. INTRODUCTION

The photodissociation of ozone is arguably the most important reaction in the photochemistry of Earth's atmosphere, as it provides a protective shield against harmful ultraviolet radiation from the Sun.^{1,2} This protection arises from efficient absorption by ozone at wavelengths between 200 and 300 nm known as the Hartley band. Radiation within this spectral range would otherwise reach the Earth's surface with detrimental effects to life, causing damage to DNA and other biomolecules.³ While the photochemistry of ozone has been studied extensively in this spectral region, its photodissociation at higher photon energies is less well-characterized, owing to the lower solar flux, coupled with the high absorption cross-section of molecular oxygen at $\lambda < 200$ nm.^{4,5} As such, ozone absorption is considered less important at these wavelengths, but ozone does have a weak, unnamed absorption band between 150 and 200 nm.^{6,7} In this study, we investigate the photodissociation of O₃ at 193.4 and 157.6 nm, with the specific goal of characterizing the 3-fragment O₃ → 3 O channel.

The photodissociation of ozone at 193 nm (6.4 eV) has been the subject of several experimental studies,^{8–13} mostly regarding the dominant O₃ → O₂ + O process. Two of these studies are of particular importance for the present work. Measurements of the quantum yield of both O(³P) and O(¹D) atoms reported in Ref. 14 revealed a quantum yield greater than unity (1.20 ± 0.15). This result was attributed to a small contribution (~12%) from 3-fragment dissociation of O₃ to form three O(³P) atoms. This dissociation pathway becomes energetically available at ~6.2 eV ($\lambda \lesssim 200$ nm) and is thus

just barely accessible at 193 nm (6.4 eV). It was also observed by photofragment translational spectroscopy⁹ at 193 nm as a very sharp feature at low translational energy. In that work, 3-fragment dissociation was estimated to be ~2% of the total fragmentation.

Ozone photodissociation at wavelengths shorter than 193 nm has received very little experimental attention. In measurements⁸ of the O atom quantum yield at 157 nm, the 3-fragment dissociation channel has been found much more prevalent than at 193 nm, constituting about half of the total fragmentation at this wavelength. It was speculated that this process occurs in two stages involving the initial formation of a triplet O₂ intermediate with internal energy higher than the O–O bond energy, which then undergoes secondary dissociation.

Theoretical work related to photoexcitation beyond the Hartley band is also very scarce.^{7,15} It is mainly devoted to the absorption cross-section and only briefly touches on the 2-fragment dissociation dynamics. Although the electronic states of O₃ lying in the relevant energy range correlate to the 3O(³P) fragments, the 3-fragment dissociation channel has not been considered so far.

Three-fragment dissociation resulting from photoexcitation, charge exchange, or collisions has been observed in other molecules, such as H₃^{16,17} and sym-triazine,¹⁸ directly or deduced from product distributions (see Refs. 19–23 for some examples). A central question in such processes is whether the dissociation occurs through a concerted pathway, in which both bonds break simultaneously, or by a sequential process, in which one bond breaks first, leaving a highly excited intermediate fragment that dissociates after some delay.¹⁹ This question is difficult to address with conventional, non-coincidence, experimental methods, as 3-fragment dissociation is not observed directly but rather inferred from measurements of only one of the fragments. However, fast-beam

^{a)}Current address: Intel Corporation, 3065 Bowers Avenue, Santa Clara, California 95054, USA.

^{b)}Author to whom correspondence should be addressed. Electronic mail: dneumark@berkeley.edu

photodissociation experiments capable of making a time- and position-sensitive measurement of all three fragments in coincidence have proven successful in gaining additional insight into 3-fragment dissociation mechanisms.^{16,24}

Although coincident measurements have been used to investigate 3-fragment dissociative recombination of the O_3^+ cation²⁵ and the Coulomb explosion of ozone $O_3 \xrightarrow{nh\nu} O_3^{3+} \rightarrow 3O^+$,²⁶ the present work is the first fast-beam coincident study of 3-fragment photodissociation of neutral O_3 . We obtained kinetic energy distributions and branching ratios between 2-fragment and 3-fragment dissociation channels at both 193.4 and 157.6 nm. With the aid of Dalitz plot analysis,²⁷ we provide evidence for a concerted 3-fragment dissociation mechanism.

II. EXPERIMENTAL

The fast-beam coincidence translational spectrometer used in this study has been described elsewhere.^{28–30} Briefly, neat O_2 at 7 bar backing pressure is expanded into a vacuum chamber through an Even–Lavie pulsed solenoid valve³¹ equipped with a DC discharge region to produce O_3^- . At the nozzle exit, the molecular beam is also intersected by a 1 keV electron beam from a home-built electron gun to increase the amount of O_3^- . Resulting anions are then electrostatically accelerated to a beam energy of 8 keV and mass-selected using a Bakker-type mass spectrometer^{32,33} that imparts negligible kinetic energy spread to the ion beam. Mass-selected ozonide is then photodetached at 400 nm (3.10 eV) with an excimer-pumped dye laser (Lambda-Physik LPX-200 and Lambda-Physik FL 3002) to produce a fast beam of neutral ozone.

Ideally, a detachment photon energy just above the electron affinity of ozone (2.10 eV³⁴) would be preferred in order to create neutral molecules with as little internal energy as possible. However, near the photodetachment threshold, the relatively weak anion photodetachment is overwhelmed by O_3^- photodissociation, which leads to $O_2 + O^-$ (and $O_2^- + O$ at $h\nu \gtrsim 2.7$ eV) fragments^{35,36} that contaminate the studied O_3 photodissociation products. Therefore, a significantly higher energy (3.10 eV), at which the photodissociation cross-section drops and detachment becomes more favorable,³⁶ was used in the present work. This higher photodetachment energy results in population of O_3 vibrational levels up to the dissociation limit (~ 1.06 eV) with a distribution determined by Franck–Condon factors between the anion and neutral, similar to the distribution seen in the photoelectron spectrum of O_3^- .³⁴

Following detachment, the remaining ions are deflected from the beam, yielding a fast beam of neutral O_3 (along with some neutral O_2 and O fragments). This neutral packet is then intersected by an ultraviolet (UV) pulse from a second excimer laser (GAM EX-50F) at either 193.4 nm (6.41 eV, ArF) or 157.6 nm (7.87 eV, F₂). Fragments from O_3 photodissociation ($O_2 + O$ or $3O$) recoil from the beam axis and strike a time- and position-sensitive detector located ~ 2 m downstream of the photodissociation region, while undissociated parent molecules are blocked by a beam block (4 mm radius) in front of the detector.

The position and arrival time of each fragment are measured in coincidence for each dissociation event with a Roentdek Hex80 delay-line anode detector.³⁷ The detector consists of a Z stack of microchannel plates (MCP) (75 mm diameter, 40:1 aspect ratio) mounted in front of an anode comprising three layers of delay lines. After an impinging particle strikes the MCP stack, the resulting electron cloud is collected by the delay lines. The difference between the arrival times of the signal pulse at the opposite ends of each line yields one dimension of the particle position, whereas the average arrival time yields the particle arrival time (delayed by a constant amount). Combining such measurements from the three layers yields the two-dimensional position and arrival time for each particle, even if several fragments hit the detector within a short time interval. The time and position resolution are estimated to be 100 ps and 100 μ m, respectively.³⁰ Based on calibration experiments using the predissociation from the $B^3\Sigma_u^-$ state of O_2 , the kinetic energy resolution ($\Delta E/E$) is measured to be $\sim 0.8\%$.³⁸

Due to the presence of the beam block and the finite size of the detector, some events with very low or high translational energies in at least one of the fragments cannot be detected, depending on their recoil directions relative to the detector. To account for these effects, all presented distributions were obtained by correcting the raw data with a detector acceptance function (DAF, see below).

III. DATA ANALYSIS

The time and position measurements yield laboratory-frame velocities of all fragments in the dissociation event, which can be easily converted to center-of-mass (COM) velocities \mathbf{v}_i . For 3-fragment dissociation, due to conservation of total momentum, the intensity distribution in the COM frame is 6-dimensional (6D) and can be considered as a function of velocity vectors of any two fragments. However, more insight into the dynamics can be gained by representing this distribution in another set of more symmetric variables. Namely, 3 degrees of freedom corresponding to COM kinetic energies

$$E_i = m_i \mathbf{v}_i^2 / 2 \quad (1)$$

of the fragments can be accounted for by 3 “energetic” variables: the kinetic energy release (KER)

$$E = \sum_{i=1}^3 E_i, \quad (2)$$

describing the total kinetic energy of the fragments, and the 2-dimensional coordinates in the Dalitz plot,²⁷ which is a convenient way to represent kinetic energy fractions

$$\varepsilon_i = E_i / E \quad (3)$$

of each fragment. The remaining 3 degrees of freedom correspond to “orientational” variables and can be described by Euler angles (the rotation angle about the photon polarization axis, the angle between the axis and the dissociation plane, and the in-plane rotation angle).

Although a strong anisotropy has been observed previously in 2-fragment photodissociation of ozone ($O_3 \rightarrow O_2$

+ O) in the Hartley band (at $h\nu \approx 5.5$ eV),³⁹ experiments at shorter wavelengths (down to 193 nm)^{9,13} have shown that at higher photon energies the anisotropy decreases and eventually changes its sign due to a contribution from a higher-lying electronic state with a different symmetry. Moreover, in the case of an unpolarized laser excitation, as in our experiments, the observed distribution is averaged over polarizations, so that the apparent anisotropy in the laboratory frame is reduced.⁴⁰ This suggests that even if the 2- and 3-fragment dissociation processes might be fairly anisotropic for each particular electronic state, the likely participation of several excited states (see below) producing different anisotropies in the dissociation and this effect of averaging over laser polarizations should lead to a relatively isotropic distribution in the measured data. Analysis of 2-fragment dissociation data in our experiments did not reveal any significant anisotropy at either of the used photon energies, suggesting that the observed 3-fragment distributions are also likely to be relatively isotropic. In addition, the small amount of data collected in the experiments ($\lesssim 2000$ 3-fragment events at each wavelength) is clearly insufficient to reliably determine the complete full-dimensional distribution and reconstruct the smeared and overlapping contributions from each particular vibrational level. Therefore, we decided to assume that the distribution is totally isotropic with respect to all “orientational” degrees of freedom, and analyzed only the 3D “energetic” distribution.

However, coincident detection of an event is possible if and only if all 3 fragments hit the sensitive area of the detector, and their trajectories depend on all the 6 kinematic parameters mentioned above. The detector acceptance function, therefore, was calculated by numerical integration in the full 6D space (using the actual geometric parameters of the setup) and over the parent beam distribution (obtained from analysis of the data) and then reduced to a 3D DAF under the assumptions of isotropic dissociation. The experimental data were binned to obtain a “raw” empirical distribution, which was then divided by this DAF to obtain an estimation of the underlying “true” (DAF-corrected) distribution.

By integrating over energy partitioning, the 3D distributions can be reduced to a kinetic energy release distribution (KER), which is 1-dimensional. In addition, the energy partitioning, either for particular KER or integrated over KERs, can be conveniently represented by 2-dimensional Dalitz plots.²⁷ Since several somewhat different diagrams are currently referred to as “Dalitz plots,” it is necessary to define the convention used in the presented work. By Dalitz plot we mean the intensity distribution plotted in barycentric coordinates as a function of kinetic energy fractions ε_i . Since $0 \leq \varepsilon_i \leq 1$, all physically meaningful points lie inside the corresponding triangle (see Fig. 2). In addition, for fragments of equal masses, conservation of the total momentum limits the available area to the inscribed circle. For dissociation into indistinguishable fragments, as in our case, the plot must have D_3 planar symmetry, which means that only one sixth part of it is unique. Nevertheless, we show the complete plots, so that all features can be seen in context, without artificial boundaries.

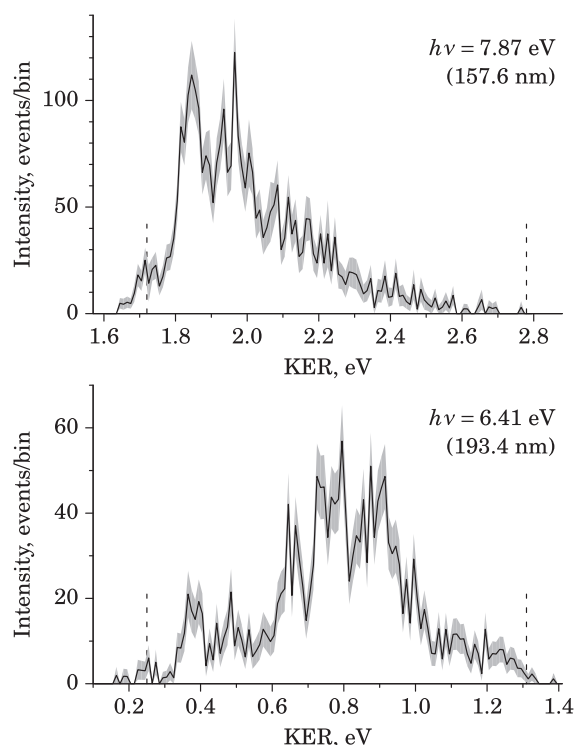


FIG. 1. Kinetic energy distributions in 3-fragment photodissociation of O_3 at 157.6 nm (top panel) and 193.4 nm (bottom panel). Bin size is 0.01 eV. Gray bands show $\pm 1\sigma$ uncertainty estimates. Dashed lines mark the center of the origin band and the upper limit of KER for photodissociation of vibrationally excited parent O_3 (determined by its dissociation energy $D_0(O_3 \rightarrow O_2 + O)$).

IV. EXPERIMENTAL RESULTS

Figure 1 shows the kinetic energy distributions obtained for 3-fragment dissociation at both excitation energies. These plots show two notable features. First, the spectra are extended and structured, even though all three fragments are atomic species. This result reflects the fact that the parent O_3 molecules are formed in a range of vibrational levels because the photodetachment energy lies well above the electron affinity of ozone. Photodissociation from each level results in a different kinetic energy release for the fragments:

$$E = h\nu - D_0(O_3 \rightarrow 3O) + E_{\text{vib,rot}}(O_3). \quad (4)$$

Hence, each peak in the spectrum can in principle be assigned to a specific vibrational level of O_3 .

At each photoexcitation energy, the vertical dashed line at low KER in Fig. 1 corresponds to photodissociation of O_3 from its ground vibrational level, while the higher-energy dashed line is offset by the maximal possible O_3 vibrational energy. As expected, all the signal lies between these two limits. Positions of the origin peaks in the KEDs measured at both photoexcitation energies are also in good agreement with the values expected from the currently known value of the dissociation energy $D_0(O_3 \rightarrow 3O) = D_0(O_3 \rightarrow O_2 + O) + D_0(O_2) \approx 6.18$ eV (using $D_0(O_3 \rightarrow O_2 + O) \approx 1.06$ eV⁴¹ and $D_0(O_2) \approx 5.12$ eV⁴²).

A second key observation is that the relative intensities of these peaks are different at 193.4 and 157.6 nm, even though the parent O_3 molecules were produced identically in all

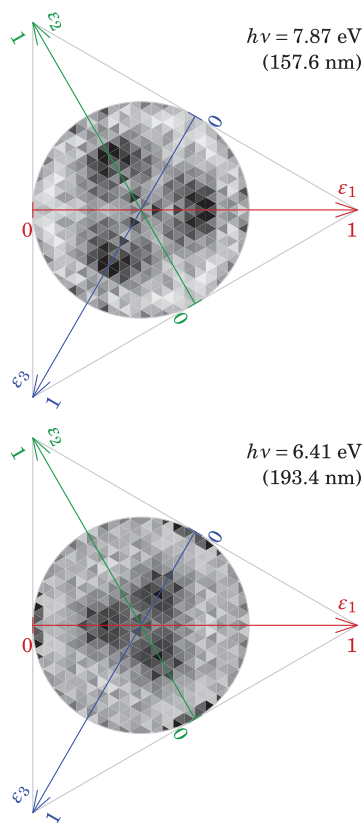


FIG. 2. Dalitz plots for 3-fragment photodissociation of O_3 at 157.6 nm (top panel) and 193.4 nm (bottom panel) integrated over the whole KER range. Relative intensities are shown by shades of gray ranging from white (no signal) to black (maximal signal).

experiments and thus must have identical vibrational level populations. This demonstrates that the initial O_3 vibrational distribution is not the sole factor governing the intensities in the KEDs. One must also consider the relative transition probabilities for electronic excitation from each vibrational level at these photon energies and the possibility that the branching ratios between 3-fragment and 2-fragment dissociation depend on both the particular initial O_3 vibrational level and the photoexcitation energy. Therefore, the observed differences between the profiles of the KEDs indicate that at the two wavelengths, photoexcitation and subsequent dissociation proceed differently.

Figure 2 shows Dalitz plots integrated over the whole KER spectrum (0.1–1.4 eV for 193.4 nm data and 1.6–2.8 eV for 157.6 nm, see Fig. 1). Due to the relatively small amount of data, even these integrated distributions have considerable shot noise (with standard deviations of intensities no less than 15%). Also, as mentioned above, the presence of the beam block causes a significant decrease in the DAF for events with very small energy in one of the fragments. This effect is responsible for the high-intensity artifact in $\epsilon_i \approx 0$ regions in the 193.4 nm plot, which in fact comes from just 5 events, greatly amplified by DAF correction.

Nevertheless, the overall structure of the distributions is evident in the plots. Although these distributions are different for the two photoexcitation energies, they have some common properties: nonzero intensities are seen for all possible energy

partitionings, but a large share of the intensity is concentrated in three spots corresponding to approximately equal fractions of energy in two of the fragments and slightly smaller (for 193.4 nm) or somewhat larger (for 157.6 nm) fraction in the other fragment.

The KEDs for 2-fragment dissociation $\text{O}_3 \rightarrow \text{O}_2 + \text{O}$ were also determined from corresponding coincident measurements; see the supplementary material.⁴³ These distributions cover a much wider KER range than the 3-fragment distributions, reflecting the much larger available energy for 2-fragment dissociation. They show no vibrational structure, owing to the combination of the initial broad distribution of O_3 vibrational levels with the presence of additional product degrees of freedom associated with the rovibrational states of the O_2 fragment. Moreover, the O_2 and O fragments are produced in multiple combinations of electronic states.⁹ No evidence of anisotropy above the noise level was observed in the distributions at either wavelength. The main utility of these data in the present work is for estimating the branching ratios between the 2- and 3-fragment channels, as discussed in Sec. V C.

V. DISCUSSION

A. Kinetic energy distributions

Since the parent O_3 molecules are created by photodetachment of O_3^- , their vibrational populations are determined by Franck–Condon factors (FCFs) for the photodetachment transition. Our experimental setup does not have the capability to measure photoelectron spectra, which would allow direct determination of the populations, but we can assume that the precursor vibrational distribution is similar to that in the previous experiments³⁴ and use corresponding FCF simulations to infer the expected O_3 vibrational distribution. They show that the noticeably larger bond lengths and a slightly smaller bond angle in O_3^- than in O_3 lead to a long progression in the symmetric stretch and some excitation of the bending mode upon detachment.

If all vibrational levels of O_3 produced by photodetachment exhibited the same 3-fragment dissociation efficiency, then the 3-fragment KEDs would be similar to the FC distribution of O_3 vibrational levels, and the KEDs at 193.4 and 157.6 nm would have identical profiles merely shifted in energy. As shown in the supplementary material,⁴³ the KED at 157.6 nm is similar to the FC distribution but shows noticeably higher relative intensity in the range 1.8–2.0 eV, which corresponds to $v_1 = 1, 2$ and combination levels with $v_2 = 1$. The KED at 193.4 nm shows little resemblance to the FC distribution, having much higher intensity beyond 0.6 eV, which corresponds to vibrational levels with $v_1 \geq 3$. The deviations of both KEDs, especially at 193.4 nm, from that expected based solely on the O_3 vibrational distribution means that we need to consider the details of the photodissociation mechanism.

Photodissociation of O_3 requires photoexcitation to one (or several) of its excited electronic states, with probabilities governed by corresponding FCFs, and subsequent break-up into three atomic fragments, which competes with

2-fragment break-up. These two factors could be separated if state-resolved branching ratios could be determined. Unfortunately, as mentioned above, in our case the 2-fragment KEDs are structureless, so that contributions from different O_3 levels overlap and cannot be resolved. On the other hand, the effect of FCFs on the photoexcitation probabilities can be estimated.

Although the potential energy surface (PES) and vibrational wavefunctions have been thoroughly studied for the ground electronic state of O_3 ,^{44,45} studies of the electronically excited states^{7,15,46–48} have been more limited. They are focused on dissociation of relatively cold molecules into $O_2 + O$, mostly at lower excitation energies that are relevant to the ozone UV absorption in the atmosphere. Thus, rigorous calculations of relevant FCFs from results available in the literature are impossible, and undertaking required electronic structure and vibrational computations is beyond the scope of the present work. Nevertheless, PES cuts along the symmetric stretch coordinate (which leads to 3-fragment dissociation) for electronic states lying in the relevant energy range have been published⁷ and can be used for rough estimation of FCF behavior with respect to the ν_1 mode. Specifically, the classical Franck–Condon principle, which states that electronic transitions are most likely to occur between classical turning points,⁴⁹ allows us to determine the extent of vibrational excitation in the ν_1 mode of the ground electronic state required to make vertical transitions to the excited electronic states possible for given photoexcitation energies.

This analysis,⁴³ which can be understood from Fig. 3, shows that while there are electronic states vertically accessi-

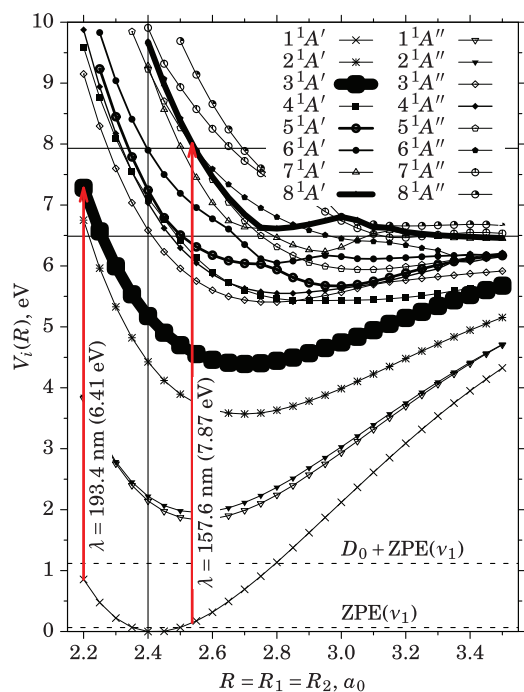


FIG. 3. PES cuts along the symmetric stretch coordinate (taken from Fig. 3 of Ref. 7) drawn with line widths proportional to vertical transition dipole moments from the ground state minimum (Table I of Ref. 7). The vertical solid line indicates the geometry of the ground state minimum, and the horizontal lines show the energies corresponding to photons with $\lambda = 193.4$ and 157.6 nm. The red vertical arrows show the most intense transitions between classical turning points for vibrationally excited O_3 .

ble near both photodissociation energies (using notation from Ref. 7: $4^1A'' (^1B_1)$ for 193.4 nm (6.41 eV) and $6^1A' (^1A_1)$ for 157.6 nm (7.87 eV)), their transition dipole moments are relatively small. For 157.6 nm, a stronger transition can occur to the $8^1A' (^1B_2)$ state at a slightly stretched nuclear configuration, requiring ~ 0.1 eV of vibrational energy, which corresponds to $\nu_1 \approx 1$. For 193.4 nm, the situation is even more remarkable. Here, the vertical transition to the $3^1A' (^1B_2)$ state, which is responsible for the strong absorption in the Hartley band, requires ~ 0.8 eV of vibrational energy, corresponding to $\nu_1 \approx 6$, and reduced bond lengths. These transitions are indicated in Fig. 3 by vertical arrows. Hence, excitation of the ν_1 vibrational mode should enhance absorption at both wavelengths, and this effect should be particularly pronounced at 193.4 nm.

In order to account for the combined effect of photodetachment and photoexcitation probabilities on the relative intensities $I(\nu_1, \nu_2, \nu_3)$ in the KEDs, the O_3 populations $N(\nu_1, \nu_2, \nu_3)$ resulting from photodetachment must be multiplied by relative photoexcitation probabilities $f(\nu_1, \nu_2, \nu_3)$:

$$I(\nu_1, \nu_2, \nu_3) \sim N(\nu_1, \nu_2, \nu_3) f(\nu_1, \nu_2, \nu_3). \quad (5)$$

As a simple approximation, we assume that the photoexcitation FCF distributions for these strongest states can be described by Gaussian functions centered at the corresponding “vertical” ν_1 values, and the overall photoexcitation probabilities to the multiple weaker states do not depend on the initial vibrational level. That is, the photoexcitation probabilities can be approximated as

$$f(\nu_1, \nu_2, \nu_3) = f_s \exp\left(-\frac{(\nu_1 - \nu_c)^2}{2w^2}\right) + f_o, \quad (6)$$

where constants f_s and f_o describe respective contributions from the strongest and from all other electronic states, ν_c is the “vertical” ν_1 value (6 for 193.4 nm and 1 for 157.6 nm), and w accounts for the width of this approximated FCF distribution for the strongest state (see the supplementary material).⁴³ We also ignore here the effects of bending and antisymmetric stretch, since they are only weakly excited in the parent O_3 . However, the bending mode might play an important role, as discussed later.

A comparison of the resulting distributions with the experimental spectra is shown in Fig. 4. As can be seen, this rough approximation is able to reproduce the overall trends in the intensities, although the intensities corresponding to combination levels $(\nu_1, 1, 0)$ with one quantum in the bending mode are substantially underestimated, especially for the $(3, 1, 0)$ and $(4, 1, 0)$ levels in the 193.4 nm distribution. It is very unlikely that the observed excess in $(\nu_1, 1, 0)$ intensities is caused by enhanced populations in O_3 , since FCF simulations for the photodetachment step do not allow selective excitation of $\nu_2 = 1$ levels without also populating $\nu_2 = 2$ levels, which do not seem to be enhanced in the experimental spectra. Therefore, the levels with bending excitation might either have higher photoexcitation probabilities at these photon energies or higher probabilities to dissociate into three fragments. These two possibilities cannot be

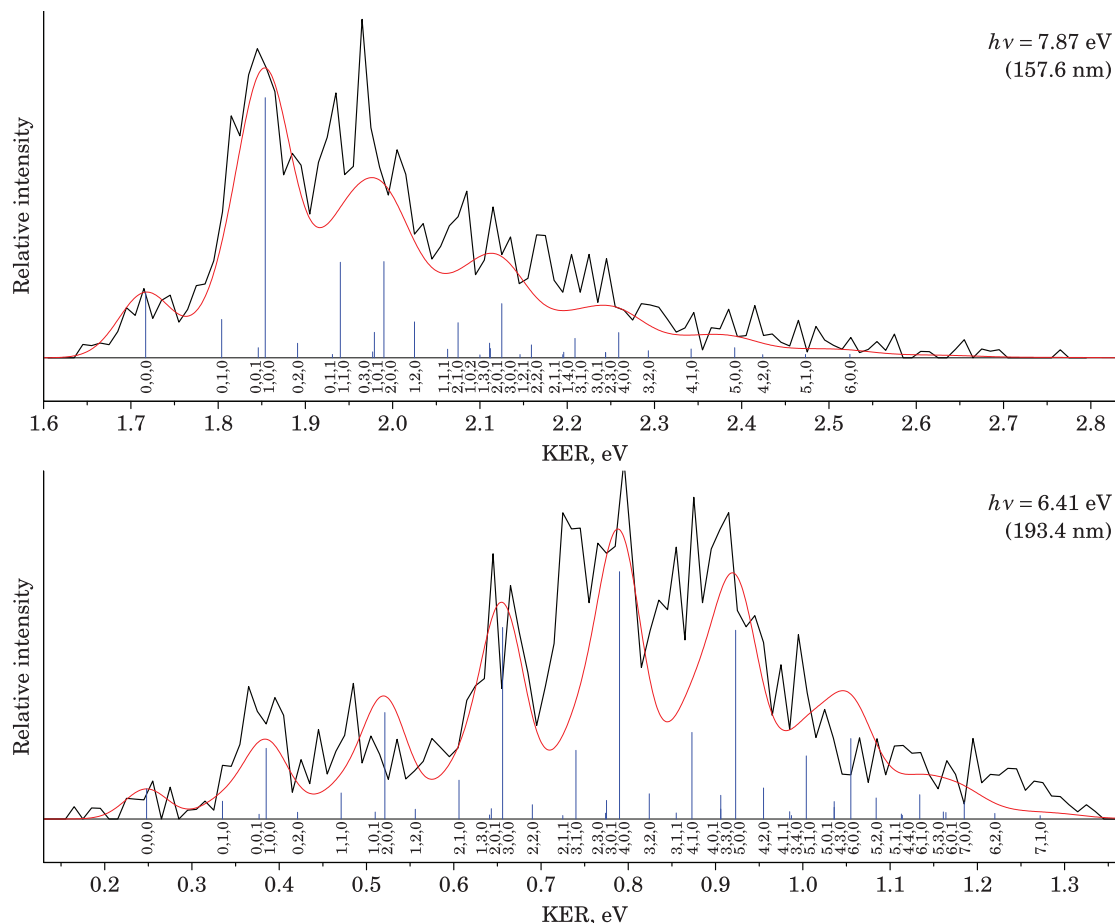


FIG. 4. Comparison of simulated intensity distributions (see text) with experimental KEDs (Fig. 1). Experimental distributions are shown by black lines, simulations by red curves, and blue sticks indicate positions and simulated intensities corresponding to individual $\text{O}_3(\bar{X}^1A_1)$ vibrational levels marked by vibrational quantum numbers v_1, v_2, v_3 (symmetric stretch, bending, antisymmetric stretch, respectively). Vibrational energies were taken from Ref. 44 (compilation of experimental data) and Ref. 50 (experimental data for high v_1 overtones), augmented with Ref. 45 (first-principle calculations) for experimentally unavailable data. Energies for several states missing in this collection were approximated by separable anharmonic extrapolation.

distinguished based on the available experimental data and calculations.

It should be noted that the observed peaks have halfwidths ~ 60 meV, almost independent of the kinetic energy, which is much broader than the experimental resolution (~ 20 meV for the highest energies) and the photodissociation laser bandwidth ($\lesssim 15$ meV^{51,52}). This broadening cannot be explained by rotational excitation, since that would require an unlikely high rotational temperature ~ 400 K and produce appreciably asymmetric peak shapes with long tails towards higher KER that are not observed in the spectra (moreover, the peaks in the photoelectron spectrum³⁴ of O_3^- produced in similar conditions were much narrower, suggesting a relatively low rotational temperature). However, if the electronically excited O_3^* can dissociate into three $\text{O}({}^3P_J)$ atoms with various combinations of spin-orbit states (each $J = 0, 1, 2$), the maximum KER difference between such channels ($3\text{O}({}^3P_2)$ and $3\text{O}({}^3P_0)$) should be about 84 meV, consistent with the observed halfwidths.

Unfortunately, the available theoretical studies of O_3 electronic states ignore the spin-orbit structure, and thus cannot provide any information (except very general constraints, such as parity) about possible product state combinations and

their relative contributions. In addition, even if such correlations can be determined for electronic states that are pure in some approximation, the actual branchings might be substantially different due to transitions among these “pure” states caused by various couplings taking place during the dissociation. These effects have been experimentally observed already for O_2 photodissociation³⁸ and can be expected to be much more complicated for O_3 with one more O atom and excitation of multiple electronic states.

Therefore, the observed broadening of the vibrational peaks is most likely due to dissociation into $\text{O}({}^3P_J)$ atoms in multiple spin-orbit states. The experimental resolution, however, is not sufficient to see these contributions separately, and the limited amount of data does not allow deconvolution.

B. Dalitz plots

Three-fragment dissociation mechanisms are usually classified according to the timing between breaking of the bonds.¹⁹ In the synchronous concerted mechanism, the bonds break simultaneously, leading to symmetric energy partitioning. In asynchronous concerted dissociation, one bond breaks

after the other with a delay comparable to the vibrational periods, producing an asymmetric but still correlated distribution. In sequential, stepwise dissociation, one fragment leaves first and the remaining part breaks into 2 fragments later on a timescale exceeding the rotational period, in which case the correlation between the 3 fragments is lost.

Dalitz plots provide a one-to-one representation of the energy partitioning and thus allow a direct visual examination of the correlations among the fragments, elucidating the underlying dissociation mechanism. Symmetric bond breaking should produce intensities on the symmetry lines of the plot, while asymmetric bond breaking generally partitions the energy unequally among all 3 fragments and thus should produce intensity off the symmetry lines. The loss of correlation in stepwise dissociation leads to intensities smeared along constant- ε_i lines, where the energy fraction ε_i of one of the fragments is determined at the first dissociation step.^{18,24,53}

As mentioned above, most of the intensity in the plots (Fig. 2) at both photoexcitation energies is concentrated in three spots. In neither case is the location of these spots very close to the partitioning corresponding to a sudden recoil along the bonds from the O₃ equilibrium geometry, which would yield almost equal fractions for all three fragments:

$$\varepsilon_{\text{terminal O}} = \frac{1}{2 + 4 \cos(\theta/2)^2} \approx 0.322, \quad (7)$$

$$\varepsilon_{\text{central O}} = 1 - 2\varepsilon_{\text{terminal O}} \approx 0.355, \quad (8)$$

where $\theta \approx 116.7^\circ$ is the bond angle.

Nevertheless, the distributions at both photoexcitation energies show only *three* spots, corresponding to equal energy fractions for two fragments, which suggests that the dissociation is synchronous concerted rather than asynchronous concerted, because in the latter case energy fractions for all three fragments are expected to be different, leading to *six* spots in the Dalitz plot. The asynchronous concerted mechanism can accidentally produce symmetric partitioning, but in the present experiment all three fragments are indistinguishable, and therefore these two cases cannot be clearly differentiated. This question can be investigated using O₃ isotopomers (e.g., ¹⁶O¹⁸O¹⁶O and/or ¹⁸O¹⁶O¹⁶O),⁴³ but would require much more elaborate experiments. More insight can be also gained from careful theoretical dynamics computations.

The difference in the location and size of the spots between the 193.4 and 157.6 nm data is likely due to participation of different electronic states in the dissociation. Namely, as indicated by FCF analysis above, photoexcitation at 193.4 nm occurs mostly to only one state, and PES plots⁷ show that this state does not interact with other states upon symmetric bond stretching and has only a small gradient in the bending coordinate. That is, the portion of the initial wavepacket that is not diverted towards 2-fragment dissociation should proceed roughly as symmetric dissociation along the bonds and resemble the sudden recoil approximation. On the one hand, the 157.6 nm photodissociation involves multiple electronic states, all of which have intersections accessible by symmetric bond stretching or bending. The dissociation dynamics therefore should be much more complicated

and might be expected to result in larger deviations from the sudden recoil and a broader final distribution.

The absence of constant- ε_i lines corresponding to sequential dissociation is not surprising, since a stepwise process would require creation of metastable O₂ fragments. In principle, the minimum of the lowest known metastable $B^3\Sigma_u^-$ state of O₂ lies only ~ 1 eV higher than the O₂ $\rightarrow 2O(^3P)$ dissociation limit, and this state predissociates to 2O(³P) fragments through coupling with several repulsive states.³⁸ Thus it should be energetically accessible in the 157.6 nm case. However, none of the studied O₃ electronic states correlates to O₂($B^3\Sigma_u^-$) + O(³P) fragments (the $B^3\Sigma_u^-$ state itself correlates to O(¹D) + O(³P)), which is ~ 2 eV above 2O(³P)), meaning that efficient excitation of such states probably requires much higher photon energies.

On the other hand, all excited states of O₃ in the relevant energy range seem to correlate to 3O(³P) fragments.⁷ Moreover, the dipole-accessible states have significant gradients along the symmetric stretch coordinate in the region of expected ground-state geometries (see Fig. 5 of Ref. 7), which means that at least immediately after photoexcitation the molecule should evolve towards symmetric 3-fragment dissociation. The potential energy surfaces, however, are not purely repulsive and have saddle points or conical intersections (appearing as avoided crossings in C_s symmetry) at sufficiently extended bond lengths. This severely complicates the subsequent dynamics, for example leading to preferential dissociation into O₂ + O instead of 3O, especially at lower photoexcitation energies. Even if the dissociation proceeds to 3 fragments, the initially symmetric wavepacket, after passing symmetrically through the region of a saddle point or a conical intersection, can be split into a symmetrized combination of two asymmetric wavepackets, resulting in less symmetric energy partitioning.

The energy partitioning obtained in the present experiments at 193.4 nm is close to 2:1:2, which is somewhat different from the approximately 4:1:4 ratio previously inferred from analysis of non-coincident measurements at this wavelength.⁹ At the same time, a coincident study²⁵ of dissociative recombination O₃⁺ + e⁻ \rightarrow 3O(³P), which corresponds to ~ 12.5 eV of excitation energy, exhibited almost 1:0:1 energy partitioning resulting from a practically linear recoil arrangement. This is an interesting result, given the initial O₃⁺ bent geometry, and differs significantly from the approximately 1:2:1 ratio obtained in the present work at 157.6 nm (~ 7.87 eV) excitation, reinforcing the conclusion that the dissociation process is very sensitive to the involved electronic states and is not straightforward.

Although the dynamics on the electronically excited PESs, and hence the energy partitioning among the fragments, can depend on the initial O₃ vibrational level, the small amount of experimental data obtained in the present study does not permit a meaningful analysis of KER-dependent Dalitz plots. An examination of Dalitz plots integrated over KER intervals corresponding to distinct peaks in the KEDs⁴³ shows only that the plots corresponding to the strongest peaks are more structured, and the plots for weaker peaks are more uniform. However, taking into account the amount of noise in these plots, such deviations from the overall Dalitz plots

(Fig. 2) cannot be considered statistically significant. Another way to correlate the energy partitioning with the KER is to compare the overall KED with the KED corresponding to events lying within the three intense spots in the Dalitz plot. If these spots are due to dissociation starting from particular vibrational levels, then the associated KED should differ from the overall KED shown in Fig. 1. However, such comparisons⁴³ also do not show any qualitative differences.

C. Branching ratios

The branching between the 2- and 3-fragment dissociation channels may also depend on the initial vibrational excitation, but this dependence cannot be discerned from the present experiments. Whereas vibrational structure in the 3-fragment data is partially resolved, the contributions from different initial O₃ vibrational levels are not distinguishable in the 2-fragment KEDs (see the supplementary material).⁴³ Thus only the total branchings can be extracted from the data.

The total branching ratios were obtained by comparing the total intensities (KEDs integrated over all energies) of the 2- and 3-fragment channels. This procedure, however, is not straightforward. First, the DAF decreases significantly for high-energy fragments. For example, at the highest observed energies in 2-fragment dissociation, only the fragments recoiling in a relatively small solid angle with $\sim 60^\circ$ aperture around the beam axis reach the detector. This means that the anisotropy distribution for high KERs cannot be determined reliably. Therefore, since the anisotropy parameter estimated from the scarce data was randomly scattered in the full allowable range, we decided to DAF-correct the 2-fragment distributions as if they were isotropic (see also Sec. III). This may have led to some systematic errors in the total intensity, but considerably reduced the random noise propagated to KEDs from the anisotropy estimations. For the 157.6 nm photodissociation, which produced a weak 2-fragment signal, the noise remained quite large even with this assumption.

Another factor that must be accounted for is that imperfect detection efficiency of each particle hitting the detector leads to different probabilities of coincident detection for 2- and 3-fragment events. Namely, if the 1-particle detection probability is p , then the probability of coincident detection of 2-fragment event is $P_2 = p^2$, and that of 3-fragment event is $P_3 = p^3$. The probability p can vary over a broad range (from ~ 0.3 to almost unity), depending on the speed, mass, and electronic state of the impacting particle, the particular type of the detector, its age and operating conditions.^{54–56} However, it can be estimated by comparing the detected number of 3-fragment coincidences with the number of events in which only 2 out of 3 fragments were detected (with probability $P_{2\text{ of }3} = 3p^2(1 - p)$). Such events can be separated from genuine 2-fragment dissociation, since in the latter case the COM of the event must lie within the parent beam, whereas in the former case the COM of the 2 detected fragments is displaced, and the momentum of the undetected third fragment can be estimated such that the 3-fragment COM lies within the beam. Unfortunately, the COM spread in the parent beam is not negligible, leading to relatively poor accuracy

of this reconstruction,⁴³ so that it does not yield useful information for analysis of 3-fragment dissociation as in Ref. 16. Moreover, a relatively large number of false coincidences, especially in the 193.4 nm data, produce a noticeable background in the reconstructed distributions. Nevertheless, the structured parts of the distributions are consistent with the coincident 3-fragment data, and the comparison of their intensities yields the value of $p = 0.6 \pm 0.05$ for 1-particle detection probability.

The branching fractions for the 3-fragment channel obtained from the total DAF-corrected intensities and this 1-particle detection probability are 5.2(6)% at 193.4 nm and 26(4)% at 157.6 nm.

In a previous study⁸ of O₃ photodissociation at 157.6 nm, the branching between 2- and 3-fragment dissociation was inferred from indirect measurements (fluorescence in a gas cell). It was estimated that, on average, dissociation of each O₃ molecule produces approximately two O atoms, which means that the O + O₂ and 3O channels have approximately equal probabilities. The 3-fragment fraction in photodissociation at 193 nm extracted from similar indirect measurements¹⁴ was $\sim 12\%$ (with a large uncertainty). In a later molecular-beam study,⁹ this fraction was estimated as $\sim 2\%$ from fitting the O atom time-of-flight spectra with a simple model for the 3-fragment distribution.

Our results are consistent with previous work in that the 3-fragment branching fraction is higher at 157.6 nm than at 193.4 nm. However, the agreement among the numbers is quite poor (even between the previous 193 nm studies). In part, this can be explained by relatively low accuracies of all the estimations. Even though the present results were obtained from direct measurements of both channels and thus can be deemed more reliable, they can still have systematic errors, mostly from the isotropy assumption. Another issue is that while all previous studies used vibrationally cold O₃, the branching ratios in the present work are essentially averaged over a very broad and peculiar vibrational distribution. Even though at 193.4 nm this averaged branching ratio is consistent with previous estimations for cold O₃ (and actually lies between them), the possibility that the branching ratios are vibrationally dependent cannot be ruled out, and thus the present numbers should be used with due caution.

VI. CONCLUSION

The work presented here is the first direct observation and dynamical characterization of 3-fragment photodissociation of the neutral ozone molecule. Although experimental evidence of this channel has been known for almost 30 years,⁸ it has received relatively little experimental and theoretical attention, despite being a very interesting case of 3-fragment dissociation into three atoms of a simple, stable molecule, directly related to real-world chemistry.

The Dalitz plots obtained here suggest that the dissociation proceeds by a concerted, and most probably symmetric, mechanism. It is also evident that excitation of the same vibrational ensemble of O₃ at different wavelengths results in different kinetic energy distributions and branching ratios.

It should be noted that the photodissociation wavelengths 193.4 and 157.6 nm were used here only because they can be easily produced at sufficiently high intensities. However, these wavelengths actually lie close to the *minima* of the O₃ absorption cross-section.⁷ Therefore, they correspond to a mixture of “hot bands” for several electronic transitions, which causes the observed enhancement of photodissociation probability for vibrationally excited ozone, especially at 193.4 nm. From this perspective, it would be very interesting to perform similar experiments at different wavelengths, corresponding to maxima of partial cross-sections, for example, at ~ 180 nm (~ 7 eV) for the strongest absorption in this region, involving the 5¹A' (¹A₁) state.

The analysis and interpretation of the present data was substantially complicated by a broad range of populated O₃ vibrational levels in our experiment. Therefore, development of a method for producing a fast beam of vibrationally cold or, better, state-selected neutral O₃ molecules is highly desirable. Since the precursor O₃⁻ anions in our experiment were sufficiently cold, near-threshold photodetachment coupled with some means to increase O₃⁻ production and to better separate O₃⁻ photodissociation byproducts from the O₃ beam would be of interest. Alternatively, measuring the kinetic energy of the photodetached electron in coincidence with photofragment detection⁵⁷ would help in resolving contributions from different vibrational levels.

The indirect evidence for producing the O(³P_J) fragments in multiple spin-orbit substates motivates more detailed investigations of this issue. This question has been already studied for O₂ photodissociation³⁸ using our experimental setup (with a slightly different detector). The peak separations in these experiments were somewhat larger due to a smaller number of possible combinations, and the signals were much stronger, allowing fitting of the contours. Nevertheless, optimization of conditions in the current experiment might make such measurements possible for O₃ photodissociation as well.

Finally, we hope that the experimental results reported in the present article will incite theoretical interest in the 3-fragment dissociation of ozone. The 193.4 nm case, involving one electronic state that is nearly isolated (at least along the symmetric dissociation route), should be amenable to computations using present-day methods. A reasonable description of 157.6 nm photodissociation with multiple interacting states might require a more complicated treatment with non-adiabatic effects, but can present an even better test case for non-trivial nuclear dynamics computations.

ACKNOWLEDGMENTS

This research was supported by the Director, Office of Basic Energy Science, Chemical Sciences Division of the U.S. Department of Energy under Contract No. DE-AC02-05CH11231.

¹H. S. Johnston, *Ann. Rev. Phys. Chem.* **43**, 1 (1992).

²S. Solomon, *Rev. Geophys.* **37**, 275, doi:10.1029/1999RG900008 (1999).

³N. J. Mason and S. K. Pathak, *Contemp. Phys.* **38**, 289 (1997).

⁴B. R. Lewis, S. T. Gibson, and P. M. Dooley, *J. Chem. Phys.* **100**, 7012 (1994).

⁵B. R. Lewis, S. T. Gibson, F. T. Hawes, and L. W. Torop, *Phys. Chem. Earth, Part C* **26**, 519 (2001).

⁶Y. Tanaka, E. C. Y. Inn, and K. Watanabe, *J. Chem. Phys.* **21**, 1651 (1953).

⁷R. Schinke and S. Yu. Grebenshchikov, *Chem. Phys.* **347**, 279 (2008).

⁸M. R. Taherian and T. G. Slanger, *J. Chem. Phys.* **83**, 6246 (1985).

⁹D. Stranges, X. Yang, J. D. Chesko, and A. G. Suits, *J. Chem. Phys.* **102**, 6067 (1995).

¹⁰K. Takahashi, N. Taniguchi, Y. Matsumi, and M. Kawasaki, *Chem. Phys.* **231**, 171 (1998).

¹¹K. Takahashi, T. Nakayama, and Y. Matsumi, *J. Phys. Chem. A* **107**, 9368 (2003).

¹²S. Nishida, F. Taketani, K. Takahashi, and Y. Matsumi, *J. Phys. Chem. A* **108**, 2710 (2004).

¹³M. Brouard, R. Cireasa, A. P. Clark, G. C. Groenenboom, G. Hancock, S. J. Horrocks, F. Quadri, G. A. D. Ritchie, and C. Vallance, *J. Chem. Phys.* **125**, 133308 (2006).

¹⁴A. A. Turnipseed, G. L. Vaghjiani, T. Gierczak, J. E. Thompson, and A. R. Ravishankara, *J. Chem. Phys.* **95**, 3244 (1991).

¹⁵M. H. Palmer and A. D. Nelson, *Mol. Phys.* **100**, 3601 (2002).

¹⁶U. Galster, P. Kaminski, M. Beckert, H. Helm, and U. Müller, *Eur. Phys. J. D* **17**, 307 (2001).

¹⁷Ch. M. Laperle, J. E. Mann, T. G. Clements, and R. E. Continetti, *Phys. Rev. Lett.* **93**, 153202 (2004).

¹⁸J. D. Savee, J. E. Mann, and R. E. Continetti, *J. Phys. Chem. A* **113**, 3988 (2009).

¹⁹Ch. Maul and K.-H. Gericke, *Int. Rev. Phys. Chem.* **16**, 1 (1997).

²⁰D. Xu, J. Huang, J. S. Francisco, J. C. Hansen, and W. M. Jackson, *J. Chem. Phys.* **117**, 7483 (2002).

²¹Y.-R. Lee, C.-C. Chen, and S.-M. Lin, *J. Chem. Phys.* **120**, 1223 (2004).

²²P. Zou, J. Shu, and S. W. North, *J. Photochem. Photobiol. A* **209**, 56 (2010).

²³N. Hobday, M. S. Quinn, K. Nauta, D. U. Andrews, M. J. T. Jordan, and S. H. Kable, *J. Phys. Chem. A* **117**, 12091 (2013).

²⁴P. E. Crider, A. W. Harrison, and D. M. Neumark, *J. Chem. Phys.* **134**, 134306 (2011).

²⁵V. Zhaunerchyk, W. D. Geppert, F. Österdahl, M. Larsson, R. D. Thomas, E. Bahati, M. E. Bannister, M. R. Fogle, and C. R. Vane, *Phys. Rev. A* **77**, 022704 (2008).

²⁶A. Matsuda, E. J. Takahashi, and A. Hishikawa, *J. Chem. Phys.* **127**, 114318 (2007).

²⁷R. H. Dalitz, *Philos. Mag.* **44**, 1068 (1953).

²⁸R. E. Continetti, D. R. Cyr, R. B. Metz, and D. M. Neumark, *Chem. Phys. Lett.* **182**, 406 (1991).

²⁹A. A. Hoops, J. R. Gascooke, A. E. Faulhaber, K. E. Kautzman, and D. M. Neumark, *Chem. Phys. Lett.* **374**, 235 (2003).

³⁰A. W. Harrison, J. S. Lim, M. Ryazanov, G. Wang, Sh. Gao, and D. M. Neumark, *J. Phys. Chem. A* **117**, 11970 (2013).

³¹U. Even, J. Jortner, D. Noy, N. Lavie, and C. Cossart-Magos, *J. Chem. Phys.* **112**, 8068 (2000).

³²J. M. B. Bakker, *J. Phys. E* **6**, 785 (1973).

³³J. M. B. Bakker, *J. Phys. E* **7**, 364 (1974).

³⁴D. W. Arnold, C. Xu, E. H. Kim, and D. M. Neumark, *J. Chem. Phys.* **101**, 912 (1994).

³⁵S. E. Novick, P. C. Engelking, P. L. Jones, J. H. Futrell, and W. C. Lineberger, *J. Chem. Phys.* **70**, 2652 (1979).

³⁶J. F. Hiller and M. L. Vestal, *J. Chem. Phys.* **74**, 6096 (1981).

³⁷O. Jagutzki, A. Cerezo, A. Czasch, R. Dorner, M. Hattas, M. Huang, V. Mergel, U. Spillmann, K. Ullmann-Pfleger, T. Weber, H. Schmidt-Bocking, and G. D. W. Smith, *IEEE Trans. Nucl. Sci.* **49**, 2477 (2002).

³⁸D. J. Leahy, D. L. Osborn, D. R. Cyr, and D. M. Neumark, *J. Chem. Phys.* **103**, 2495 (1995).

³⁹R. L. Miller, A. G. Suits, P. L. Houston, R. Toumi, J. A. Mack, and A. M. Wodtke, *Science* **265**, 1831 (1994).

⁴⁰R. N. Zare, *Mol. Photochem.* **4**, 1 (1972).

⁴¹B. Ruscic, R. E. Pinzon, M. L. Morton, G. von Laszewski, S. J. Bittner, S. G. Nijsure, K. A. Amin, M. Minkoff, and A. F. Wagner, *J. Phys. Chem. A* **108**, 9979 (2004).

⁴²P. C. Cosby and D. L. Huestis, *J. Chem. Phys.* **97**, 6108 (1992).

⁴³See supplementary material at <http://dx.doi.org/10.1063/1.4882644> for 2-fragment kinetic energy distributions, Franck-Condon simulations, detailed Dalitz plots, and reconstruction of 3-fragment distributions from 2 detected fragments for determination of branching ratios.

⁴⁴V. I. G. Tyuterev, S. Tashkun, P. Jensen, A. Barbe, and T. Cours, *J. Mol. Spectrosc.* **198**, 57 (1999).

⁴⁵R. Siebert, P. Fleurat-Lessard, R. Schinke, M. Bittererová, and S. C. Farantos, *J. Chem. Phys.* **116**, 9749 (2002).

- ⁴⁶S. Yu. Grebenshchikov, Z.-W. Qu, H. Zhu, and R. Schinke, *Phys. Chem. Chem. Phys.* **9**, 2044 (2007).
- ⁴⁷R. Schinke and G. C. McBane, *J. Chem. Phys.* **132**, 044305 (2010).
- ⁴⁸H. Han, B. Suo, D. Xie, Y. Lei, Y. Wang, and Z. Wen, *Phys. Chem. Chem. Phys.* **13**, 2723 (2011).
- ⁴⁹E. Condon, *Phys. Rev.* **28**, 1182 (1926).
- ⁵⁰B.-Y. Chang, C.-Y. Kung, C. Kittrell, C.-W. Hsiao, B. R. Johnson, S. G. Glogover, and J. L. Kinsey, *J. Chem. Phys.* **101**, 1914 (1994).
- ⁵¹T. R. Loree, K. B. Butterfield, and D. L. Barker, *Appl. Phys. Lett.* **32**, 171 (1978).
- ⁵²C. J. Sansonetti, J. Reader, and K. Vogler, *Appl. Opt.* **40**, 1974 (2001).
- ⁵³A. Matsuda, M. Fushitani, R. D. Thomas, V. Zhaunerchyk, and A. Hishikawa, *J. Phys. Chem. A* **113**, 2254 (2009).
- ⁵⁴D. de Bruijn, P. van Deenen, D. Dijkkamp, H. Holsboer, and C. van Oven, *Microchannel Plate Report* (FOM-Instituut voor Atoom- en Molecuulfysica, Amsterdam, 1982), Chap. 1.
- ⁵⁵M. Barat, J. C. Brenot, J. A. Fayeton, and Y. J. Picard, *Rev. Sci. Instrum.* **71**, 2050 (2000).
- ⁵⁶B. Brehm, J. Grosser, T. Ruscheinski, and M. Zimmer, *Meas. Sci. Technol.* **6**, 953 (1995).
- ⁵⁷B. L. J. Poed, Ch. J. Johnson, and R. E. Continetti, *Faraday Discuss.* **150**, 481 (2011).